scientific reports

Check for updates

OPEN

Integration of network pharmacology, transcriptomics, and experimental verification to investigate the mechanism of action of cepharanthine hydrochloride against prostate cancer

Zongming Dong[1,4], Xiaosa Chang[1,4], Xing Luo[1,4], Hui Li[2], Ming Deng[1], Zeyu Huang[1], Tingting Chen[1], Yu Chen[1], Bishao Sun[1], Yingbing Wu[1], Ronghua Wu[1], Qingjian Wu[1], Jingzhen Zhu[1]✉ & Ji Zheng[1,3]✉

The incidence of prostate cancer (PCa) is high among elderly men. Cepharanthine hydrochloride (CH) is recognized for its important role in the prevention and treatment of various diseases. However, its effects and mechanisms of action in the context of PCa remain unclear. Our study aims to examine the therapeutic role and mechanisms of action of CH in PCa. Targets of CH and PCa-related genes were identified using different databases, and the biological processes through which CH might exert its therapeutic effects were predicted via protein–protein interaction (PPI) network and enrichment analyses. Subsequently, the PCa cell lines PC-3 and DU145 were used to assess the concentration- and time-dependent effects of CH on cell viability, proliferation, and migration. Transcriptomic sequencing and differential expression analysis were used to identify the key target protein of CH and the key signaling pathways involved in its therapeutic effects against PCa. Molecular docking was used to analyze the binding between CH and its target protein. Additionally, quantitative reverse transcription polymerase chain reaction (qRT-PCR), western blotting, gene knockout, pharmacological intervention, and tumor formation experiments were performed to validate the therapeutic effects and mechanisms of action of CH against PCa in vitro and in vivo. Network pharmacology showed that CH, a Chinese herbal medication, might prevent PCa by regulating protein phosphorylation-related biological processes. In vitro experiments showed that CH inhibited the proliferation and migration of PCa cells in a concentration-dependent manner. In addition, integration of transcriptomic sequencing, differential expression analysis, and GO enrichment analysis suggested that the ERK protein played a crucial role in the anti-tumor activity of CH. Molecular docking and molecular dynamics simulations revealed strong binding affinities between CH and ERK1/2. Further experimental verification, involving qRT-PCR, western blotting, gene knockout, pharmacological intervention, and tumor formation experiments, demonstrated that CH upregulated dual-specificity phosphatase (DUSP) 1 and suppressed the phosphorylation of ERK, thereby inhibiting the development and progression of PCa in vivo and in vitro. In conclusion, the findings of this study suggest that CH suppresses the ERK signaling pathway by enhancing the expression of DUSP1, thereby exerting anti-tumor effects against PCa in vitro and in vivo. Therefore, CH may serve as a novel therapeutic agent for PCa, showing remarkable potential for clinical application.

Keywords Cepharanthine hydrochloride, Prostate cancer, Mechanism investigations, Network pharmacology, Transcriptomics, Molecular docking

Abbreviations

ADT	Androgen deprivation therapy
BP	Biological processes
CC	Cellular components
CH	Cepharanthine hydrochloride
CSPC	Castration-sensitive prostate cancer
CTB	Compound–target–biological process
DUSP	Dual-specificity phosphatase
FBS	Fetal bovine serum
GO	Gene ontology
MAPK	Mitogen-activated protein kinase
MKPs	MAPK phosphatases
MF	Molecular functions
PARP	Poly ADP-ribose polymerase
PCa	Prostate cancer
PMSF	Phenylmethanesulfonyl fluoride
PPI	Protein–protein interaction
PSMA	Prostate-specific membrane antigen
PTEN	Phosphatase and tensin homologue
SD	Standard deviation
TCM	Traditional Chinese medicine

[1]Department of Urology, Urologic Surgery Center, Xinqiao Hospital, Third Military Medical University (Army Medical University), Chongqing 400037, China. [2]Department of Ultrasound, Xinqiao Hospital, Army Medical University, Chongqing 400037, China. [3]State Key Laboratory of Trauma and Chemical Poisoning, Third Military Medical University (Army Medical University), Chongqing 400042, China. [4]Zongming Dong, Xiaosa Chang, and Xing Luo contributed equally to this work. ✉email: zhujz1114@tmmu.edu.cn; jizheng@tmmu.edu.cn

Prostate cancer (PCa) is the most common malignant tumor in the male urinary system. More than 299,010 new cases of PCa are reported annually in the United States of America[1], whereas approximately 134,200 new cases of PCa are reported annually in China, making it the sixth most common tumor among Chinese men. During the past two decades, the incidence of PCa has shown a steady increase worldwide[2]. Owing to its metastability and insidious onset with an exceptionally long incubation period, PCa is typically diagnosed at an advanced stage (III or IV), eliminating the possibility of surgical resection for complete recovery. Other treatment modalities, such as radiotherapy, chemotherapy, and chemical castration with androgen deprivation therapy (ADT), offer limited therapeutic benefits and are associated with high recurrence rates[3,4]. To date, several studies have focused on developing novel therapies for PCa, especially castration-sensitive prostate cancer (CSPC), such as poly ADP-ribose polymerase (PARP) inhibitor therapy, prostate-specific membrane antigen (PSMA)-targeted therapy, and immunotherapy[5–9]. Altogether, it is necessary to identify effective drugs that can provide optimal clinical benefits to patients with PCa.

As a mainstream form of complementary and alternative medicine, traditional Chinese medicine (TCM) is widely used to treat cancer because of its beneficial effects and minimal side effects. Cepharanthine hydrochloride (CH), a semi-synthetic derivative of cepharanthine with high solubility, bioavailability, and stability, is a bisbenzylisoquinoline alkaloid derived from the root of *Stephania cephalantha* v. hayata[10]. CH possesses various pharmacological properties and has been used in the clinical treatment of several chronic and acute diseases for decades[11–13]. It was initially used in Japan to treat patients with severe pulmonary tuberculosis and markedly reduced mortality in these patients[14]. Subsequently, several studies reported its novel pharmacological properties, including anti-inflammatory, antioxidant, and bone-protective properties[15–17]. Notably, recent studies have shown that cepharanthine may reverse the dysregulation of most genes and pathways in COVID-19-infected cells, suggesting that cepharanthine is a promising therapeutic option for COVID-19[18,19]. In addition, cepharanthine has been shown to exhibit anti-tumor activity in various cancer types. For instance, it can arrest the cell cycle in G1 and S phases and induce chromatin condensation and nuclear fragmentation in liver cancer (HuH-7) cells[20]. It mediates apoptosis by upregulating p21Waf1/Cip1 and downregulating cyclin A and Bcl-2 in colorectal cancer cells[21]. Moreover, it suppresses AKT/mTOR to induce autophagy in breast cancer (MCF-7 and MDA-MB-231) cells[22]. Recent molecular studies have supported the potential of cepharanthine as a novel chemotherapeutic drug for cancer[23]. Given that CH holds substantial promise as an anti-tumor agent, understanding its therapeutic role and mechanism of action is an important avenue for further cancer research.

In this study, we integrated network pharmacology, transcriptomic sequencing, and in vitro and in vivo experimental verification to investigate the effects and mechanism of action of CH against PCa. According to the results of network pharmacology, CH may protect against PCa by participating in phosphorylation-related biological processes. Furthermore, CH inhibited the viability, proliferation, and migration of two common PCa cell lines, PC-3 and DU145. Transcriptomic analysis showed that ERK and the DUSP family were involved in the anti-tumor effects of CH. Molecular docking validated the binding between CH and ERK1/2. Experimental verification demonstrated that CH enhanced DUSP1 expression and suppressed ERK signaling to inhibit the growth of PCa cells. Knockout and pharmacological inhibition of DUSP1 partially reversed the toxic effects of CH on PCa cells. In addition, CH significantly suppressed tumorigenesis in nude mice with subcutaneous tumors. Overall, we comprehensively investigated the mechanism of action of CH against PCa at the molecular level using network pharmacology, transcriptomics, molecular docking and experimental validation in *vitro* and in *vivo*.These findings indicated that CH might be a potential drug for the treatment of PCa.

Materials and methods

Obtaining targets of CH and PCa

Drug target prediction for CH firstly involved obtaining the SMILES of CH from PubChem (https://pubchem.ncbi.nlm.nih.gov/). Subsequently, in order to identify the targets of CH, the SMILES was respectively inputted into the Swiss Target Prediction database (http://www.swisstargetprediction.ch/), Super-PRED database (https://prediction.charite.de/index.php), and Pharmmapper database (http://lilab-ecust.cn/pharmmapper/). For PCa target prediction, PCa-related targets were obtaind through screening in the DisGeNET database (https://www.disgenet.org/home/), GeneCards database (https://www.genecards.org/), OMIM database (https://www.omim.org/), and TTD database (http://db.idrblab.net/ttd/).

Network pharmacologic analysis

Using Venny 2.1 (http://bioinfogp.cnb.csic.es/tools/venny/), we generated a Venn diagram to identify interaction targets between CH and PCa. Subsequently, we constructed a protein–protein interaction (PPI) network with a confidence level exceeding 0.7 utilizing the STRING online tool (https://string-db.org). We then performed Gene Ontology (GO) enrichment analysis by importing the overlapping genes into the DAVID online platform (https://david.ncifcrf.gov), which resulted in the identification of the top 20 biological processes (BP), cellular components (CC), and molecular functions (MF). Finally, we constructed a drug-target-biological process network by using Cytoscape v3.7.2 software.

Cell lines and cell culture

The prostate cancer cell lines PC-3 and DU145, as well as the normal human prostatic epithelial cell line RWPE-1, were procured from Shanghai Zhong Qiao Xin Zhou Biotechnology Co., Ltd. and identified by STR analysis. PC-3 and DU145 lines were cultured in RPMI-1640 medium (Gibco, USA), supplemented with 10% Fetal Bovine Serum (FBS) (Gibco, USA), 1% penicillin, and 1% streptomycin (Gibco, USA). RWPE-1 cells were maintained in keratinocyte serum-free medium (K-SFM) (Zhong Qiao Xin Zhou, China), which is supplemented with 0.05 mg/ml bovine pituitary extract (BPE), 5 ng/ml human recombinant epidermal growth factor (EGF), 10% fetal bovine serum (Gibco, USA), and additionally fortified with 1% penicillin and 1% streptomycin (Gibco, USA). Cell lines were maintained at 37 °C in a humidified incubator supplied with 5% CO_2. CH was purchased from Chengdu MUST Bio-technology Co., Ltd (Purify: HPLC > 95%) and dissolved in DMSO (Sigma, USA) to obtain a 10 mM stock solution. The cells were treated with DMSO as a negative control. BCI (MedChemExpress, USA) was dissolved in DMSO.

Cell proliferation assay

CCK-8 proliferation assays were performed to detect the anti-tumor activity of CH against PC-3 and DU145 cells, according to the manufacturer's instructions (Beyotime, China). Briefly, cells were placed into 96-well plates (Coring, USA) (2×10^3 cells/well) with 100 μL of medium. Different concentrations of CH (0, 2.5, 5, and 10 μM) were added to each well. After 0, 24, 48, 72, and 96 h of incubation, 10 μL CCK-8 regent was mixed with cells and unceasingly incubated for 1 to 2 h. Finally, the absorbance at the wavelength of 450 nm of every well was evaluated by a MultiSkan GO microplate reader (Thermo, USA).

Cell migration assay

Cell motility was evaluated using scratch and transwell assays. Scratch assay was performed by Culture-Insert 2 Well (Ibidi, Germany). 70 μL cell suspension (5×10^5 cells/mL) was added to each well and CH (0, 5, and 10 μM) was mixed. The Culture Inset was removed after incubation for 24 h and unceasingly incubated for 12, 24, and 48 h in medium without FBS. Transwell assay was performed using 24-well transwell chambers and 8μM pores (Corning, USA). In the upper chamber, 200 μL of the cell suspension (1×10^6 cells/mL) was placed with 2% FBS and different concentrations of CH (0, 5, and 10 μM), and 600 μL of medium with 10% FBS was placed in the lower chamber. After incubation for 48 h, the upper chamber was removed and the cells were washed three times with PBS. The cells were fixed with 4% paraformaldehyde and staining with crystal violet.

Cell cycle and apoptosis assays

Cells were treated with different concentrations of CH (0, 5, and 10 μM) for approximately 48 h. The cells were digested with trypsin (Gibco, USA) and washed twice with precooled PBS. Then the cells were resuspended with 70% ethanol and immobilized at 4 °C overnight. The cells were stained with PI and RNase for 30 min at room temperature in the dark. Finally, the DNA content was analyzed using a flow cytometer (BECKMAN, USA). Apoptotic cells were detected using the Annexin V PE/7-AAD apoptosis detection kit (Beyotime, China) following the manufacturer's instructions. After treatment with CH (0, 5, and 10 μM) for approximately 48 h, the cells were digested with trypsin and washed three times with pre-cooling PBS. Then the cells were strained with 10 μL Annexin V/PE and 10 μL 7-AAD at room temperature for about ten minutes at dark place. The stained cells were detected using a flow cytometer (BECKMAN, USA).

RNA isolation, transcriptome sequencing, and differential analysis

After incubation with 0 or 5 μM CH for 72 h, PC-3 cells were collected and washed with PBS. The collected samples were digested using TRIzol™ reagent (Invitrogen, USA). Total RNA was extracted using chloroform, isopropyl alcohol, 75% ethanol, and DEPC H_2O, following the manufacturer's protocol. Transcript library construction and sequencing were performed by LC-bio (China). Raw reads were filtered to obtain clean reads. The mRNA levels of the transcripts and genes were assessed according to fragments per kilobase of transcript per million mapped reads (FPKM). Based on the FPKM, different expression analyses of PC-3 with DMSO or

5 μM CH were executed and subsequently used for Kyoto Encyclopedia of Genes and Genomes (KEGG)[24] and Gene Ontology (GO) annotations.

Molecular docking

The protein crystal structures of both ERK1 (PDB ID: 6GES) and ERK2 (PDB ID: 6G54) were downloaded from the PDB database (https://www.rcsb.org/). The chemical structure of CH was obtained from the pubchem website (https://pubchem.ncbi.nlm.nih.gov/). The CID (Compound Identifier) of CH was 102,241,901 and the CAS number was 6014-83-1. The AutoDock Tools was then used to prepare the ligands and proteins required for molecular docking. The protein structures were preprocessed and optimised prior to docking, in which the amino acids in the loop region were supplemented, missing amino acid residues were added, and the intramolecular hydrogen bonding network was optimised. In this process, water molecules and small co-crystallized molecules that could affect the experimental results were removed from some irrelevant crystals. The location of the original active molecule was defined as the binding site, and was used to generate the docking box. The binding site residues used as grid centers are numbered as follows: Thr202/Tyr204 for ERK1; Thr185/Tyr187 for ERK2. Further docking was implemented by using AutoDock Tools and performed 50 times. Finally, pymol was used to generate the picture.

Quantitative real time (qRT)-PCR assay

After extracted from PC-3 and DU145 cells, 1 μg RNA was used to synthesize cDNA using PrimeScript™ RT reagent Kit (TaKaRa, Japan) according to the manufacturer's protocols. The cDNA was used for PCR amplification using SYBR Premix Ex Taq™ II (TaKaRa, Japan) on a Stepone Plus real-time PCR system (Applied Biosystems, USA). The mRNA expression levels were finally determined by comparison with those of Actin. Each sample was tested in triplicate and three independent experiments were performed. All primers used in this study are listed in Table S1.

Western blot assay

The total protein from cells with DMSO or 5 μM CH exposure was extracted by NP-40 lysis buffer containing 1% protease inhibitor, Phenylmethanesulfonyl fluoride (PMSF) (Beyotime, China). The protein concentration was determined using a BCA Protein Assay Kit (Beyotime, China). The expression of target proteins was identified via western blot using the following antibodies: anti-BAX, anti-Bcl-2, anti-Bcl-xl, anti-Mcl-1, anti-Tubulin, anti-JNK, anti-p-JNK, anti-P38, anti-p-P38, anti-GAPDH (Proteintech, China), anti-ERK, anti-p-ERK (Beyotime, China), and DUSP1 (Abclonal, USA). Prior to antibody incubation, we cropped the membranes based on the molecular weight of the target proteins to focus on specific regions of interest.

Gene knockout assay

CRISPR system was used to knock out DUSP1 in this study by electroporation instruments (DAKEWE, China). The sgRNAs were designed using the CRISPick system (https://portals.broadinstitute.org/gppx/crispick/public) and the target sequences are as follows: for DUSP1-sgRNA1, the sequence is 5′-CAGTACCCCACCTCT ACGATC-′, and for DUSP1-sgRNA2, the sequence is 5′-AAGCGTGATACGCACTGCCC-3′. 2 × 10^6 cells were gathered and centrifuged. The cell mass was resuspended in a buffer solution. The Cas9 protein (Thermo, USA) and sgRNA were incubated for 20 min at 4 °C. The cells were then incubated for 5 min. The mixture was transferred into electroporation instruments and electrocuted at 420 V, 20 ms. The mixture was then transferred into a 12-well plate for normal culture.

In vivo tumor formation assays

All BALB/c-Nude mice were sourced from Beijing Vital River Laboratory Animal Technology Co., Ltd. All animal handling and experimental protocols were carried out in accordance with the Guide for the Care and Use of Laboratory Animals, and approved by the Laboratory Animal Welfare and Ethics Committee of the Army Medical University, China (approval no. AMUWEC2020186). All efforts were made to minimize animal suffering and to reduce the number of animals used. 12 male nude mice (4 weeks) were used in our experiments. Approximately 2 × 10^6 PC-3 cells were subcutaneously injected into each mouse. Seven days after tumor-bearing mouse model construction, 30 mg/kg CH was injected into each mouse once every 3 days, while DMSO was injected into negative control mice. After four weeks, the tumor volume and weight were measured. These mice were euthanized by sodium pentobarbital injection.

Molecular dynamics

Molecular dynamics simulations were performed by using the gromacs software. Firstly, the protein structural complex was prepared, atom groups are selected and defined, the CHARMM36 force field was opted, then SPC water model was selected and then solvents and ions were introduced to equilibrate the system. Heating was simulated for 4 ps, heating occurred at 2 fs intervals, and intermediate results were saved at 2 ps intervals. The starting temperature (K) for the heating simulation was 50.0 K, and the target temperature (K) for the heating phase was 300 K. A molecular dynamics simulation was performed for 100 ns. The NVT ensemble was kept at a constant number of particles, constant volume, and constant temperature. An energy-minimizing NVT equilibrium is then performed. At the end of the simulation, the conformations were acquired, the results were generated, the kinetic simulation trajectories were analyzed, obtained complex ligands after MD simulations and analyze hydrogen bonding and the root-mean-square fluctuation (RMSF), root-mean-square deviation (RMSD) and radius of gyration of the protein backbone and small-molecule ligand during the simulation process were calculated.

Statistical analysis

All data were expressed as mean ± standard deviation (SD). Statistical analyses were performed with SPSS software (version 26.0) and graphs were generated using GraphPad Prism (version 8.0). Comparison of data before and after sample processing was performed using paired t-tests, comparison of data between multiple groups was performed by using one-way ANOVA, and further comparisons between two groups were performed using the least significant difference method. Differences between groups were assessed using the MannWhitney U test for non-normally distributed data. Differences were considered statistically significant at $P < 0.05$.

Results

Network pharmacological analysis of CH

Natural compounds often interact synergistically with multiple biochemical pathways and targets, contributing to their intricate mechanisms of action. Network pharmacology, a widely used bioinformatic approach, enables the investigation of drug–disease relationships, prediction of potential drug targets, and exploration of mechanisms of action of drug[25]. Consequently, in this study, we used network pharmacology to evaluate the therapeutic efficacy of CH in PCa and designed subsequent experiments based on the results.

After eliminating duplicates, we identified 368 targets of CH from the Pharmmapper, Swiss Target Prediction, and Super-PRED databases and 6160 PCa-related genes from the DisGeNET, GeneCards, OMIM, and TTD databases. The two gene sets were intersected, resulting in the identification of 213 core genes (Fig. 1A, Tables S2–S3). As shown in Fig. 1B, the protein–protein interaction (PPI) network of the core genes contained 210 nodes and 2645 edges. This analysis revealed that several key targets associated with PCa, including EGFR, SRC, AKT1, PIK3CA and NFKB1 were centrally positioned within the network. Several studies have demonstrated these proteins have been shown to play an important role in the development and progression of PCa.

To elucidate the potential mechanism of action of CH against PCa, the 213 core genes were subjected to GO enrichment analysis, which included three domains, namely, biological processes (BPs), molecular functions (MFs), and cellular components (CCs) (Fig. S1A). The top 10 BPs involved in the therapeutic action of CH against PCa are shown in Fig. 1C. In particular, the core genes were most significantly enriched in BPs related to phosphorylation and protein phosphorylation (Fig. 1C, Table S4), which implied that these processes might play a central role in the treatment of CH on PCa. Followed by those related to signal transduction, negative regulation of the apoptotic process, and positive regulation of cell proliferation. Finally, we visualized the PPI network and the results of GO enrichment analysis using the Cytoscape software and constructed a compound–target–biological process (CTB) network (Fig. 1D). Altogether, the results highlighted the potential of CH as a novel drug for treating PCa.

CH inhibited PCa cell viability in a concentration-dependent manner

To validate the therapeutic efficacy of CH in PCa, We first determined the IC50 values for cells RWPE-1, DU145, and PC-3 (Fig. S1B–D). Meanwhile, we used docetaxel as a positive drug control (Fig. S1E,F). we evaluated the impact of different concentrations and exposure times of CH on the viability of PC-3 and DU145 cells using CCK-8 assay. The results showed that treatment with CH significantly inhibited the viability of PC-3 and DU145 cells, with PC-3 cells exhibiting higher susceptibility than DU-145 cells to 2.5 μM CH (Fig. 2B). Morphological analysis revealed that PC-3 cells appeared round after treatment with 5 μM or 10 μM CH, whereas control cells exhibited a spindle shape with a high refractive index. On the contrary, no such changes were observed in DU145 cells (Fig. 2C, left). Assessment of mitochondrial signaling showed that CH decreased the mitochondrial membrane potential in a concentration-dependent manner (Fig. 2C, middle). Furthermore, Hoechst 33,342 staining of the nucleus indicated increased karyopyknosis with increasing concentrations of CH (Fig. 2C, right). The morphological differences between PC-3 and DU145 cells indicated that PC-3 cells were more sensitive to CH.

Apoptosis is an important mode of programmed cell death and is involved in the response of cancer cells to several drugs. We performed annexin V PE/7-AAD double staining assay to assess whether CH induced apoptosis in PCa cells. In the control, 5 μM CH, and 10 μM CH groups, the average apoptosis rates of DU145 cells were 2.46%, 4.26%, and 8.29%, respectively, whereas those of PC-3 cells were 4.2%, 7.18%, and 7.42%, respectively (Fig. 2D, E). Subsequently, western blotting was performed to examine changes in the expression of several apoptosis-related proteins. The results showed that CH increased the protein expression of BAX and decreased the protein expression of Bcl-2, Bcl-xl, and Mcl-1, indicating that CH remarkably promoted PCa cell apoptosis (Fig. 2F, G). Altogether, the results showed that CH led to morphological transformation of PCa cells, inhibited cell proliferation, and induced cell apoptosis.

CH suppressed PCa cell migration

Tumor cell migration is an important indicator of tumor progression. In this study, wound healing and transwell assays were performed to evaluate the effects of CH on the migratory ability of PCa cells. Wound healing assay showed that CH suppressed the migration of DU145 and PC-3 cells (Fig. 3A). After 24 h or 48 h of treatment, the cells in the negative-control group covered most of the scratched area, whereas the migration of both DU145 and PC-3 cells in the CH treatment groups was remarkably inhibited. After 48 h of treatment, the inhibitory effects on cell migration were stronger in the 10 μM CH group than in the 5 μM CH group. Similarly, transwell assay showed that the number of cells that penetrated the transwell insert membrane prominently decreased in a concentration-dependent manner after 48 h of treatment with CH (Fig. 3B). These results demonstrated that CH significantly suppressed the migratory ability of PCa cells.

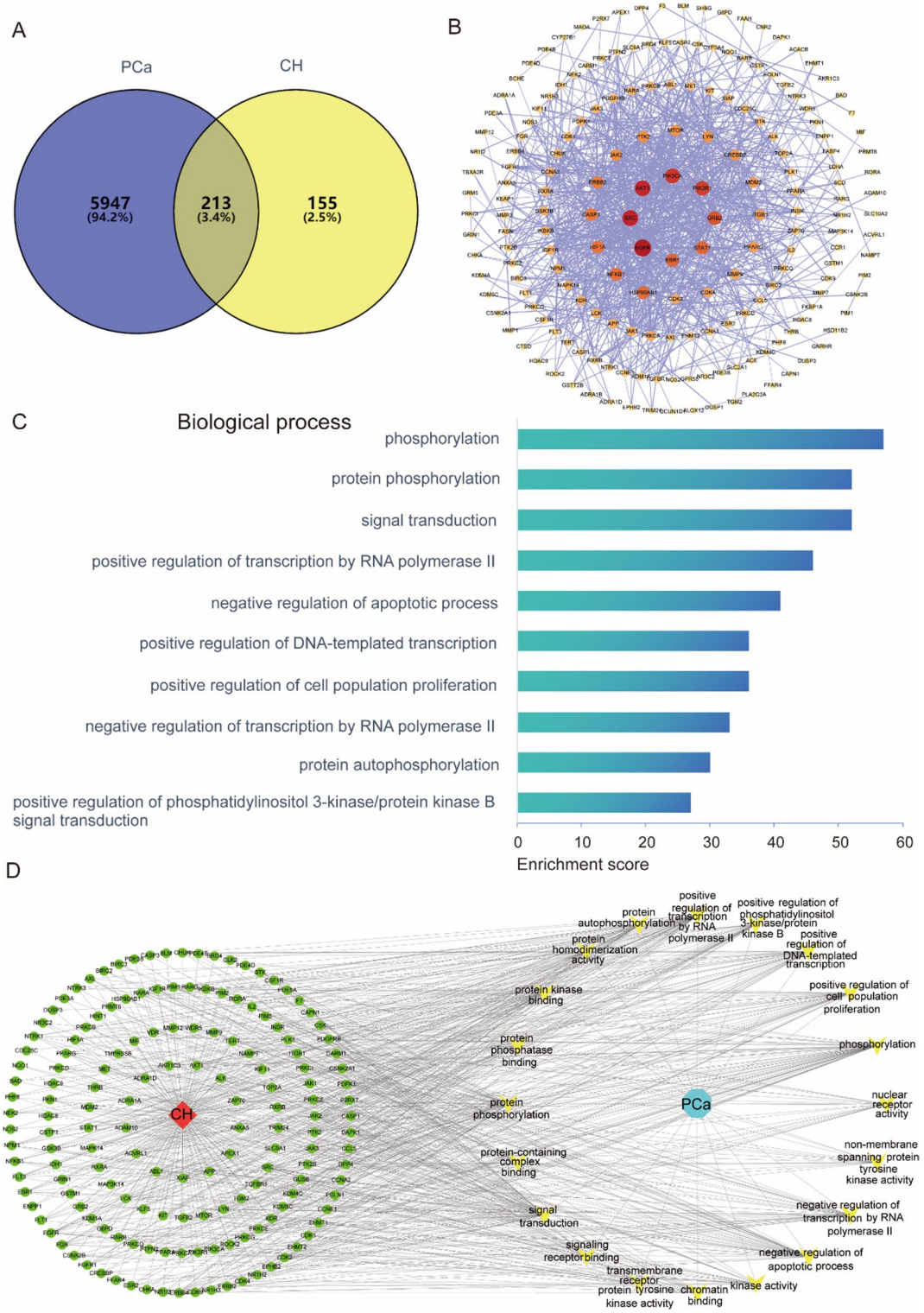

Fig. 1. Results of network pharmacological analysis of CH in PCa. (**A**) Venn diagram demonstrating the intersection between targets of CH and PCa-related genes. (**B**) A PPI network of overlapping genes was analyzed using the Cytoscape software. (**C**) Potential biological processes (BPs) involved in the mechanism of action of CH against PCa. (**D**) A compound–target–biological process (CTB) network was constructed and analyzed using STRING and Cytoscape, respectively.

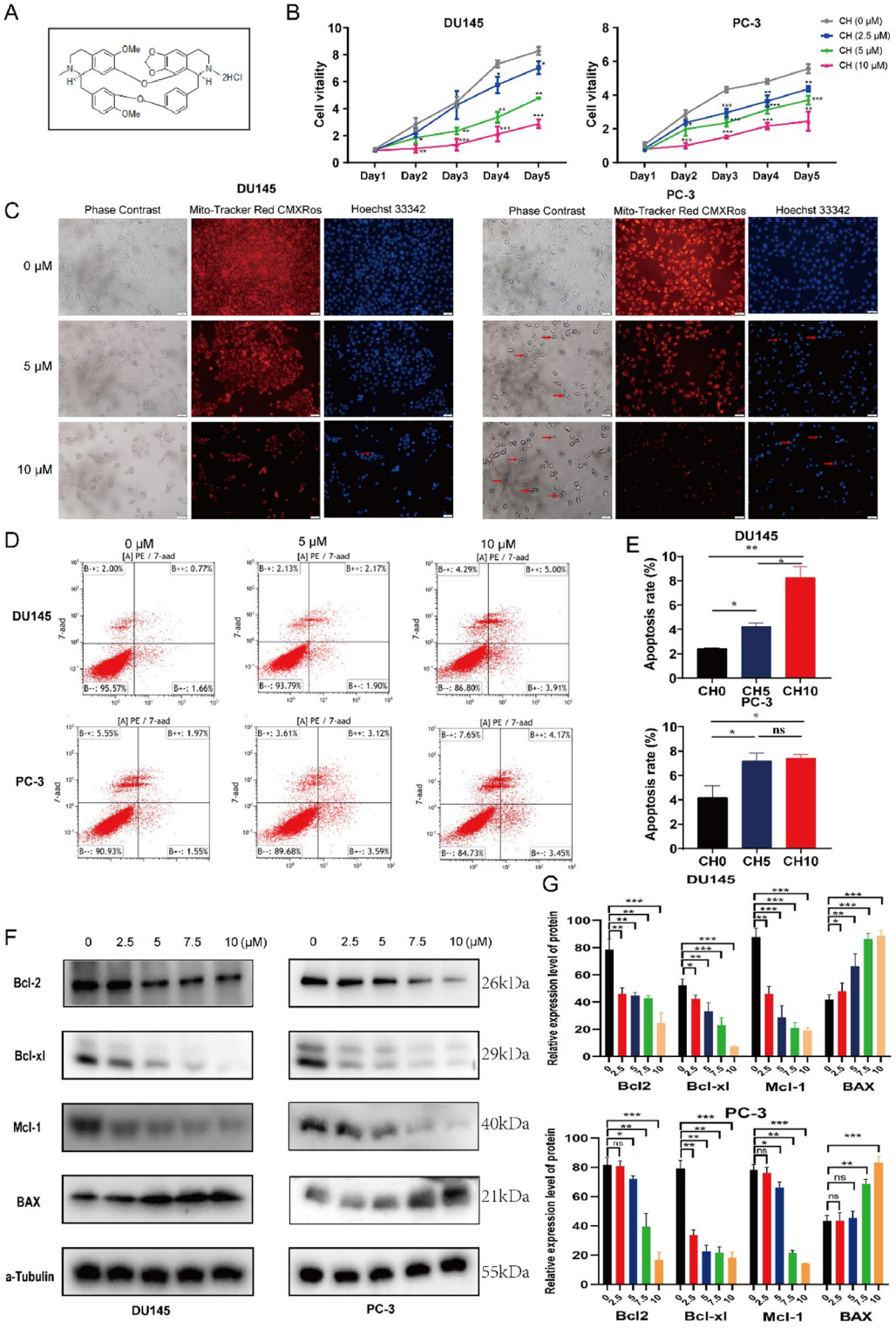

Fig. 2. CH inhibited PCa cell viability and promoted apoptosis in a concentration-dependent manner. (**A**) Molecular structure of CH. (**B**) The viability of DU145 and PC-3 cells treated with CH was evaluated via CCK8 assay. (**C**) Morphological features of DU145 and PC-3 cells treated with CH and stained with Mito-Tracker Red CMXRos and Hoechst 33,342. (**D**,**E**) The apoptosis rates of DU145 and PC-3 cells were analyzed via flow cytometry after 48 h of treatment with CH. (**F**,**G**) Western blotting was performed to evaluate the protein expression of Bcl-2, Bcl-xl, Mcl-1, and BAX. Alpha-tubulin was used as the internal reference gene. Note: *, $P < 0.05$; **, $P < 0.01$; ***, $P < 0.001$ versus the negative-control group.

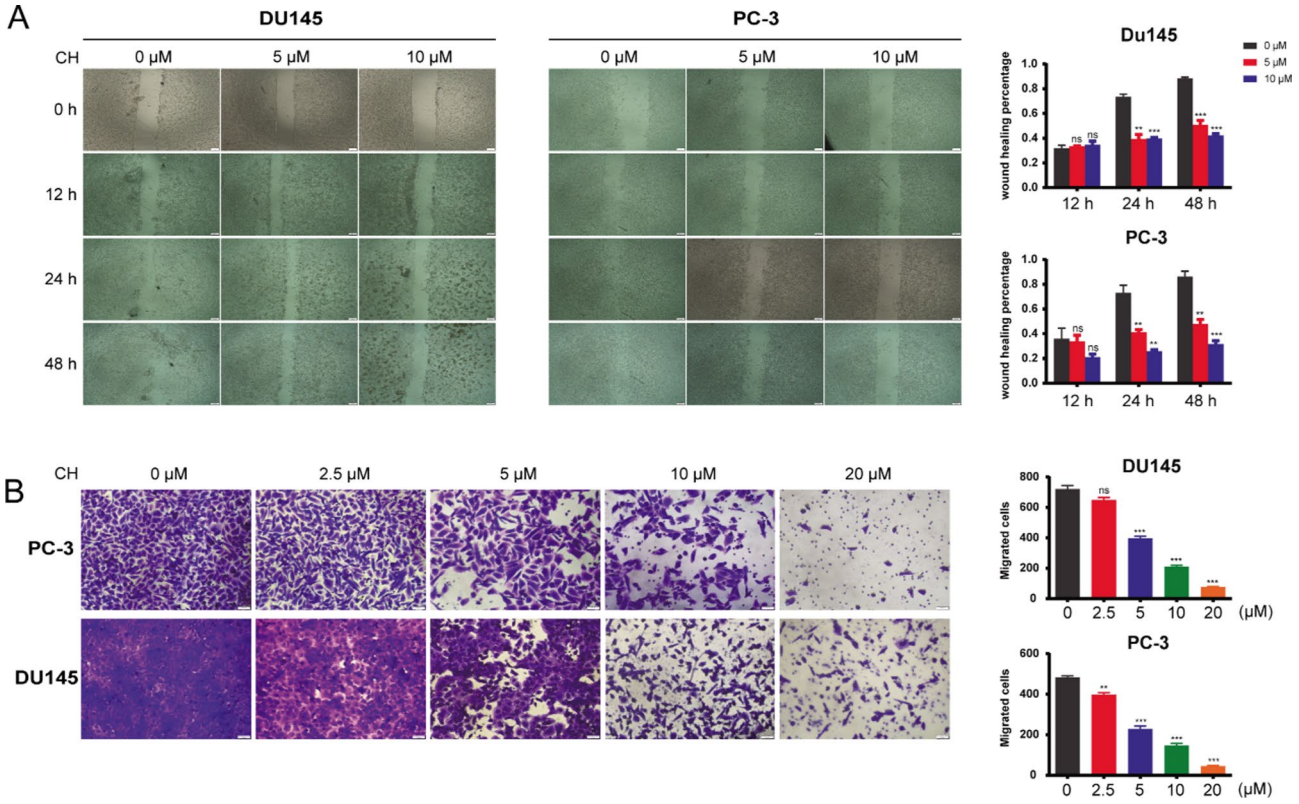

Fig. 3. CH suppressed the migration of DU145 and PC-3 cells. (**A**) Wound healing assay was performed to assess the migratory ability of DU145 and PC-3 cells treated with CH for different time points. (**B**) Transwell assay was performed to assess the migratory ability of DU145 and PC-3 cells treated with varying concentrations of CH. Note: *, $P<0.05$; **, $P<0.01$; ***, $P<0.001$ versus the negative-control group.

Transcriptomic sequencing, differential expression analysis and molecular docking

To gain further insights into the mechanism of action of CH against PCa, we performed transcriptomic sequencing on PC-3 cells treated with CH or DMSO (negative control) for 72 h. Each group of cells was analyzed in triplicate. Pearson correlation coefficients (R^2) indicated a high degree of consistency among biological replicates and substantial differences between the CH and DMSO groups (Fig. 4A). Differentially expressed genes (DEGs) between the two groups were screened based on the following criteria: corrected *P*-value (padj) < 0.05 and | log2 (fold change) value > 0. A total of 1273 DEGs, comprising 539 upregulated and 734 downregulated genes, were identified through pairwise comparisons between the CH and DMSO groups (Fig. 4B, C). A heatmap demonstrating the DEGs was shown in Fig. 4D. Similar numbers of upregulated and downregulated genes indicated that CH had similar inhibitory and activation effects on gene transcription.

Furthermore, DEGs were mapped to the KEGG database[24] and functionally annotated via GO analysis (Fig. 5). The upregulated genes in the CH group showed significant enrichment in pathways related to rheumatoid arthritis, NOD-like receptor signaling, cell cycle, legionellosis, and p53 signaling (Fig. 5A). On the contrary, the downregulated genes were enriched in pathways related to protein digestion and absorption, salivary secretion, ECM–receptor interactions, neuroactive ligand–receptor interactions, and cAMP signaling (Fig. 5B). These pathways may be involved in the mechanism of action of CH against PCa. Based on the *P*-value, the top 5 GO terms significantly enriched by the DEGs were extracellular matrix, collagen-containing extracellular matrix, extracellular matrix structural constituent, extracellular matrix organization, and angiogenesis (Fig. 5C). Importantly, based on the rich factor, the second most significantly enriched term was negative regulation of ERK1 and ERK2 cascade. ERK1 and ERK2 were well-known that regulated various cellular activities, including proliferation, differentiation, apoptosis, and stress response through phosphorylation of substrates[26].

Based on the results of network pharmacology, we speculated that CH might negatively regulate ERK and influence protein phosphorylation in PCa. To verify this speculation, we evaluated the potential regulatory relationship between CH and ERK1 or ERK2 via molecular docking. As a result, the docking score of CH with ERK1/2 were −4.579and −4.15 kcal/mol, respectively. Furthermore, we found that CH tightly occupied ATP-binding site of ERK1/2. The molecular structure was anchored in the ERK1 kinase hinge region, two aspartic acid residues (Asp128 and Asp166) of ERK1 formed hydrogen bonds with the NH groups of CH, respectively, the benzene ring of Tyr130 in ERK1 formed π–π stacking interactions with that of CH, and the Lys168 residue of ERK1 formed cation-π interactions with the benzene ring of CH (Fig. 5D). In addition, the Tyr47, Ile48 Arg84, Leu187, Val205, and Ala206 residues of ERK1 formed hydrophobic interactions with CH around the active pocket. With regard to the CH–ERK2 docking complex, the results demonstrated similar binding interactions

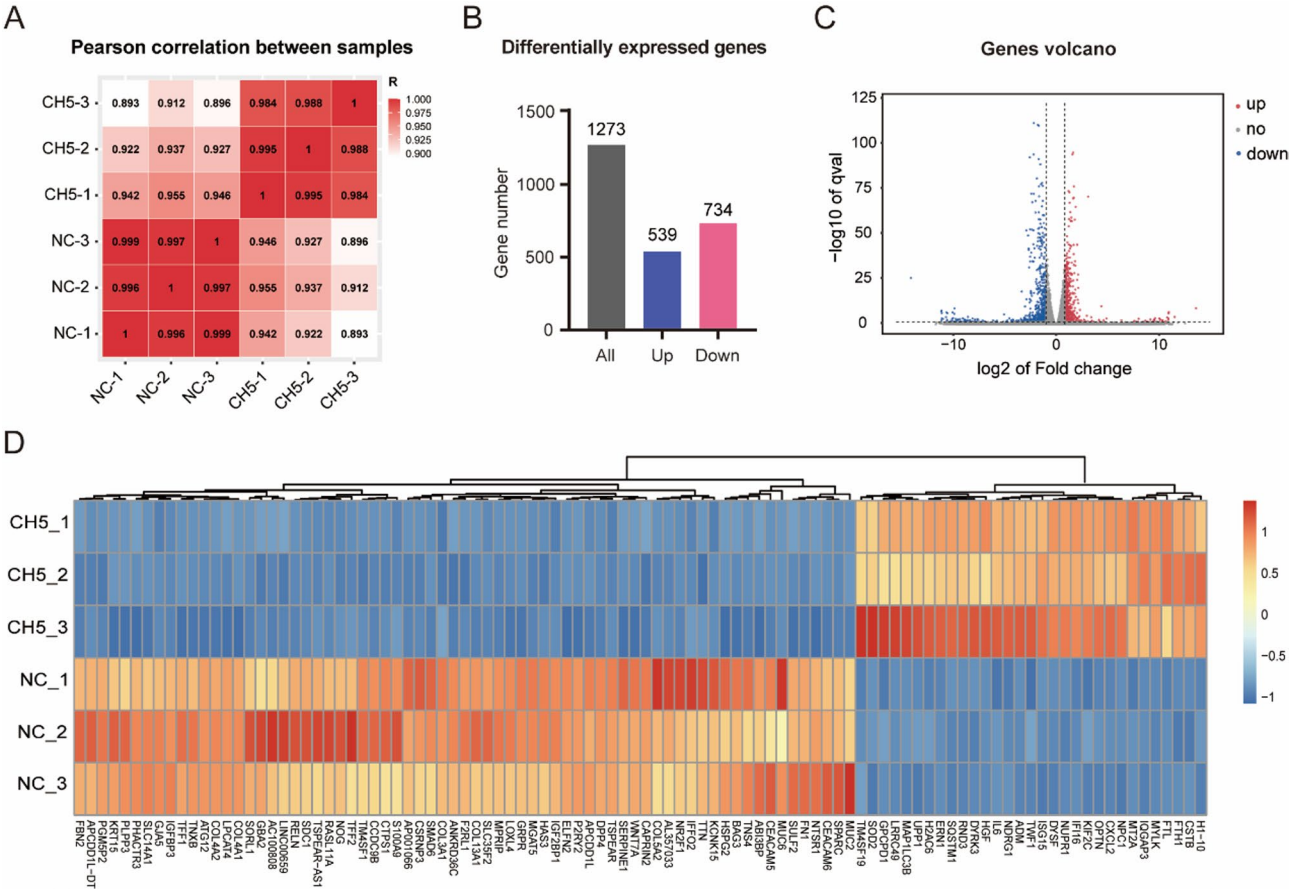

Fig. 4. Results of transcriptomic sequencing and differential expression analysis. (**A**) Pearson correlation analysis between samples. (**B**) Differentially expressed genes. (**C**) Volcano plot of differentially expressed genes. (**D**) Heatmap of differentially expressed genes.

(Fig. 5E), which may be attributed to the fact that the amino acid sequences of ERK1 and ERK2 are 80% similar. In particular, in the ATP-binding pocket hinge region of ERK2, the Asp111 and Asp149 residues of ERK2 formed key hydrogen bonds with CH; the Tyr113 residue of ERK2 formed π–π stacking interactions with CH; the Lys168 residue of ERK2 formed cation-π interactions with CH; and the Ala35, Tyr36, Leu170, and Ala189 residues formed hydrophobic interactions with CH around the active pocket. Altogether, these results demonstrated the potential binding between CH and ERK1/2, highlighting the regulatory effects of CH on the proteins.

We simulated the molecular dynamics of protein–ligand complexes after molecular docking to study the stability of CH binding to ERK proteins. The root-mean-square deviation (RMSD) value indicated the deviation of the initial conformation of the structure at a specific moment in time, and therefore reflected the stability of the system during the simulation. As shown in Figure A, CH binding to ERK1 appeared to be more inclined to be stable than the ERK2 system, and the bourgeon squared fluctuation (RMSF) analysis identified amino acid flexibility throughout the simulation. The effects of CH/ERK1 and CH/ERK2 on the amino acids of the proteins showed similarities. The overall fluctuation of the system was moderate with low RMSF values for residues between 125 and 160, corresponding to the active pocket binding pocket region. This suggested a stable interaction between the binding pockets of CH and ERK (Fig. S5A, B). We further analyzed the hydrogen bons of the complexes after md simulation, and the results showed that the number of hydrogen bonds of ERK1-CH is significantly more than that of ERK2-CH (Fig. S6A, B). On the other hand, the radius of gyration is another method used to assess the stability of protein structure. A smaller radius of gyration indicates a denser and more stable structure. The calculated average radius of gyration values of the complexes showed that the average radius of gyration of ERK1-CH protein was 1.8914, and the average radius of gyration of ERK2-CH protein was 1.9268 (Fig. S6C), which suggested that the protein-bound structure of CH and ERK1 is more stable than that of ERK2, and that the combined results of the molecular dynamics simulations suggested that the protein binding of CH and ERK1/2 is more stable. These findings might be supportive of further experimental studies.

CH inhibited ERK phosphorylation in PCa cells

The ERK1/2 pathway is located downstream of the mitogen-activated protein kinase (MAPK) signaling pathway, and its aberrant activation is closely related to tumorigenesis. Therefore, ERK signaling has emerged as a promising therapeutic target for cancer[4,28]. In addition to ERKs, the other two major components of the MAPK pathway are c-Jun amino (N)-terminal kinases 1/2/3 (JNK1/2/3) and p38. In this study, network pharmacological

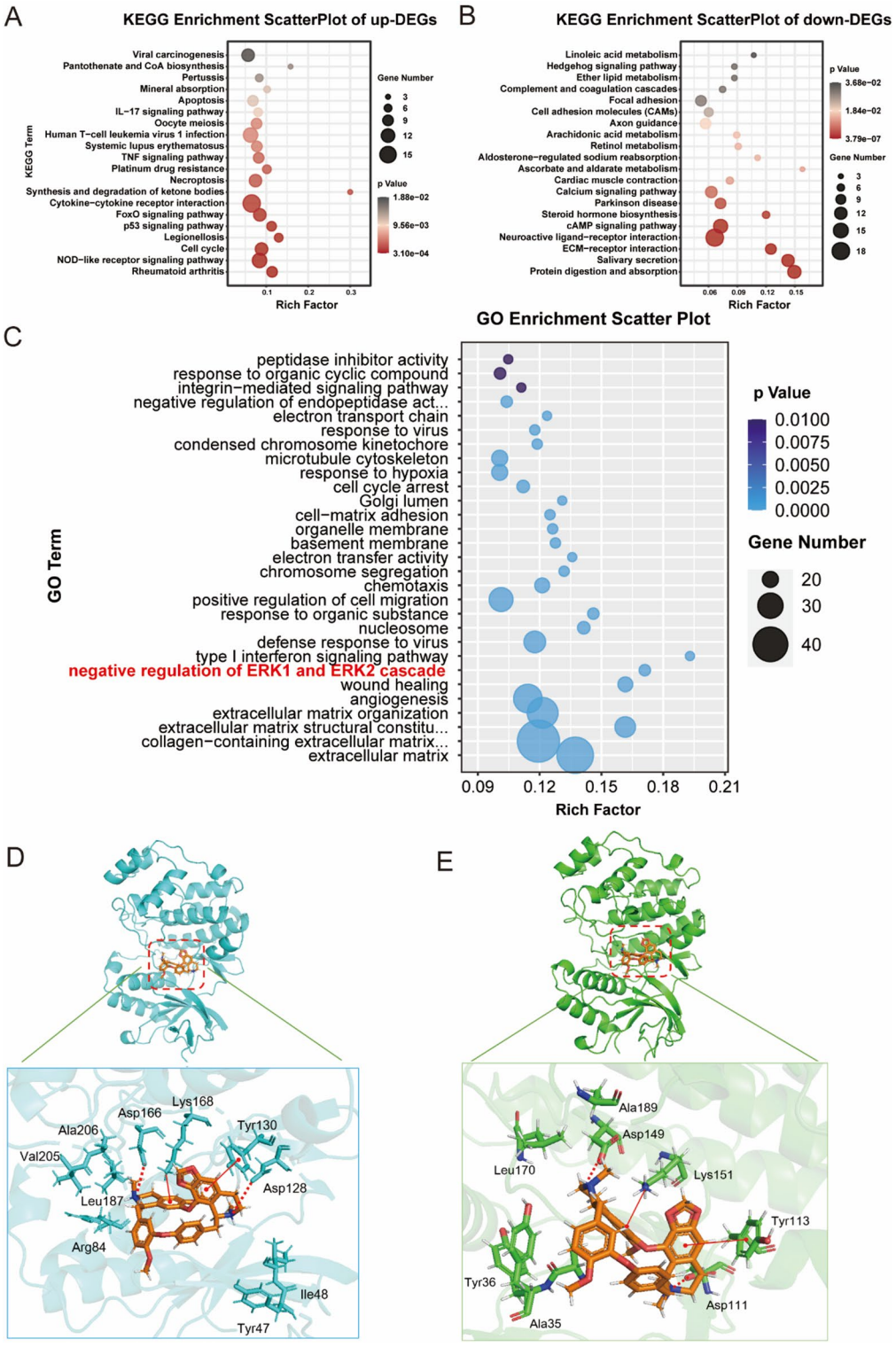

Fig. 5. Results of GO and KEGG enrichment analyses of DEGs. (**A–B**) KEGG enrichment analysis of upregulated and downregulated genes in PC-3 cells treated with CH compared with negative-control cells[24]. (**C**) GO enrichment analysis of DEGs. (**D**,**E**) Key interactions between CH and ERK1 or ERK2 based on molecular docking (ERK1 PDB ID: 6GES; ERK2 PDB ID: 6G54). Brown represents CH, whereas cyan and green represent amino acid residues of ERK1 and ERK2, respectively. The dashed lines represented hydrogen interactions, whereas the solid lines represent conjugation interactions.

analysis showed that CH might exert inhibitory effects on the development and progression of PCa through phosphorylation-related biological processes. Moreover, GO analysis suggested that DEGs between the CH and DMSO groups were associated with the negative regulation of ERK1 and ERK2 cascades (Fig. 5C).

To examine the role of ERK1/2, JNK1/2/3, and p38 in the mechanism of action of CH against PCa, western blotting was performed on PC-3 cells. The results showed that treatment with CH markedly inhibited p-ERK and p-JNK but had minimal inhibitory effects on p-p38 (Fig. 6A). Subsequently, we treated the cells with CH for a shorter period to accurately verify the timing of regulation (Fig. 6B). The results showed that CH subsequently decreased the expression of p-ERK at 0.25 h. Similar results were obtained for DU145 cells (Fig. S2), indicating that CH influenced the MAPK pathway by inhibiting phosphorylation.

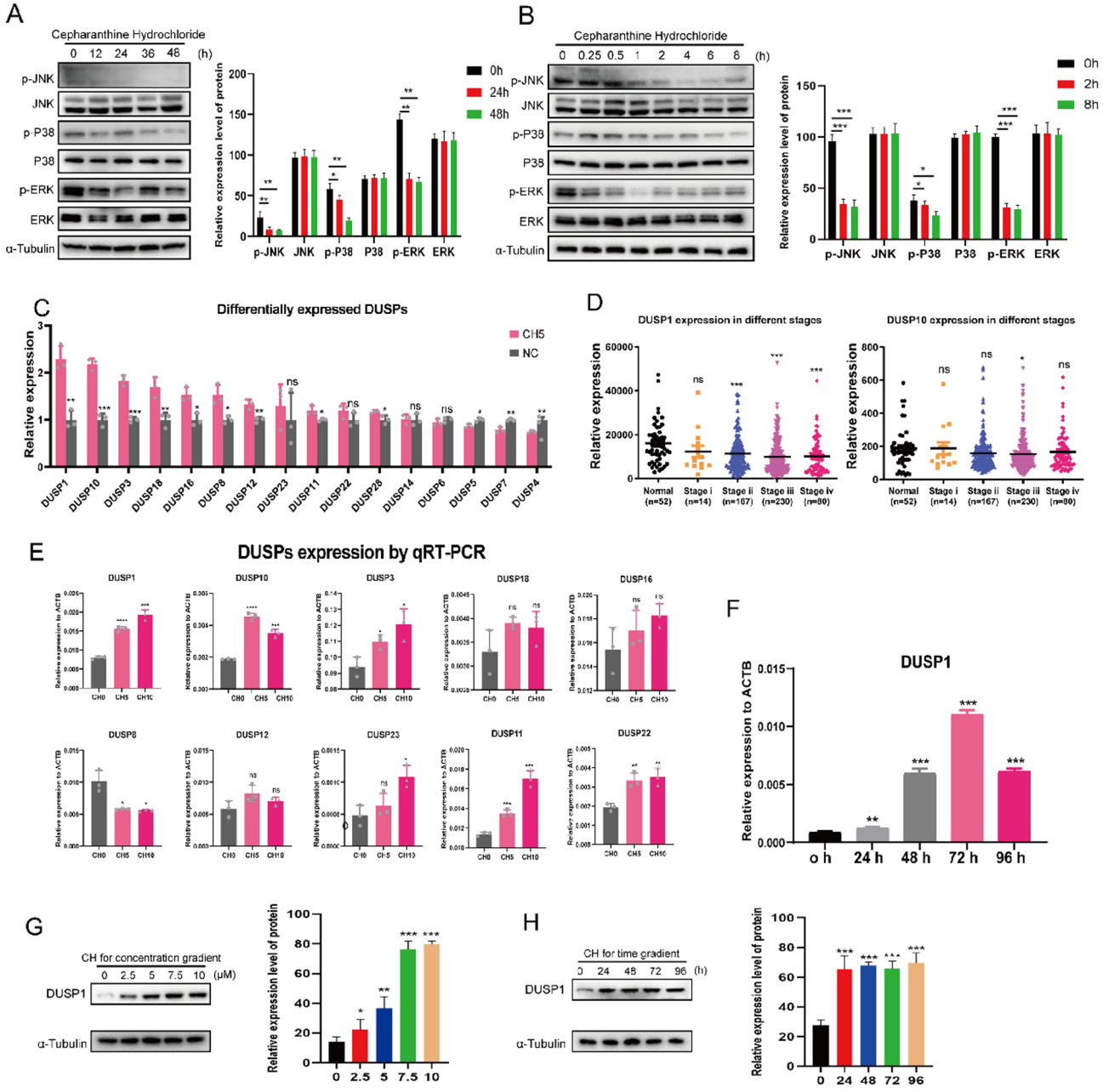

Fig. 6. CH inhibited MAPK signaling and enhanced the expression of DUSPs. (**A**) Effects of CH on MAPK signaling in PC-3 cells over a longer period of treatment. (**B**) Effects of CH on MAPK signaling in PC-3 cells over a shorter period of treatment. (**C**) Differential expression of DUSPs between the CH and negative-control groups. (**D**) Expression of DUSP1 and DUSP10 in different stages of PCa. (**E**) The mRNA expression of 10 DUSPs was evaluated via qRT-PCR. (**F**) mRNA expression of DUSP1 after treatment with CH for different time points. (**G**,**H**) Concentration- and time-dependent changes in the protein expression of DUSP1 after treatment with CH. Note: *, $P<0.05$; **, $P<0.01$; ***, $P<0.001$ versus the negative-control group.

Based on the results of western blotting and GO enrichment analysis, we investigated the mechanisms through which CH inhibited ERK phosphorylation in PCa cells. The results showed that dual-specificity phosphatase 1 (DUSP1) and dual-specificity phosphatase 10 (DUSP10) were significantly upregulated after treatment with CH (Fig. 6C, Table S5). DUSPs are a class of enzymes that dephosphorylate proteins involved in signal transduction pathways, thereby regulating important pathways related to cellular metabolism, carcinogenesis, epigenetics, and survival. To examine the role of the DUSP family in PCa cells exposed to CH, we assessed the DUSP expression profile in the cell transcriptome (Fig. 6C). A total of 16 DUSPs with obvious transcription were identified in PC-3 cells, with 12 DUSPs being upregulated after treatment with CH. In particular, DUSP1, DUSP10, and DUSP3 exhibited the strongest upregulation, with DUSP1 and DUSP10 showing a > twofold increase in expression (Fig. 6C). Subsequently, qRT-PCR was performed to evaluate the mRNA expression of 10 DUSPs in PC-3 cells treated with two different concentrations of CH (5 μM and 10 μM) (Fig. 6E). The mRNA expression of most DUSPs was upregulated after treatment with CH, with DUSP1 and DUSP10 showing particularly significant upregulation. These results validated not only the accuracy of the transcriptomic sequencing data but also the activation of the DUSP family in response to CH. The notable upregulation of DUSP1 and DUSP10 in DU145 cells strongly suggested the capability of CH to activate DUSPs in PCa (Fig. S2A). Given that DUSPs are potential therapeutic targets for cancer, we evaluated the expression of DUSP1 and DUSP10 in different stages of PCa (Fig. 6D). The results showed that DUSP1 expression was significantly lower in the PC-3 cell group than in the normal group and was negatively correlated. The expression of DUSP10 was slightly lower in the PC-3 cell group. However, the mRNA and protein expression levels of DUSP1 were consistently upregulated after treatment with CH (Figs. 6F–H, S2B–D). These results suggested that DUSP1 was most likely involved in the CH-induced inhibition of p-ERK, highlighting its potential as a novel therapeutic target for PCa.

DUSP1 was involved in CH-induced downregulation of p-ERK

To investigate the role of DUSP1 in CH-induced downregulation of p-ERK, DUSP1 was knocked out and pharmacologically inhibited in PC-3 cells. For a highly efficient knockout of DUSP1, we used the CRISPR system and designed two sgRNAs (Fig. 7A). The knockout efficiency was evaluated after 72 h of transfection with the Cas9 protein and sgRNA. Western blotting demonstrated that both sgRNA1 and sgRNA2 efficiently inhibited

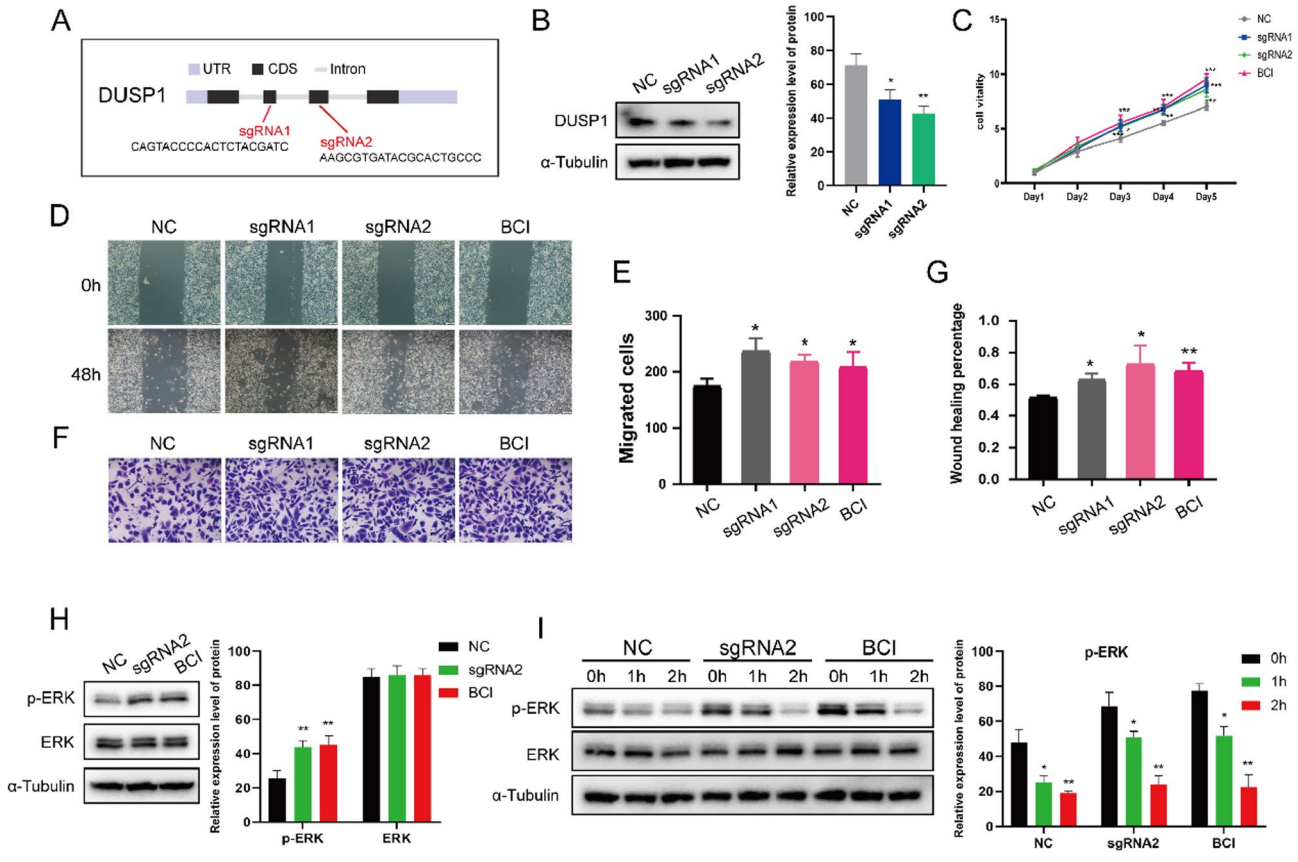

Fig. 7. DUSP1 was involved in the mechanism of action of CH against PCa. (**A**) sgRNAs targeting DUSP1 and their target sites. (**B**) Western blotting was used to evaluate DUSP1 protein expression. (**C**) Knockout and inhibition of DUSP1 counteracted the inhibitory effects of CH on PCa cell viability. (**D–G**) Knockout of DUSP1 rescued cell migration inhibited by CH. (**H**) Knockout and BCI-induced inhibition of DUSP1 promoted p-ERK signaling in PC-3 cells. (**I**) Knockout and BCI-induced inhibition of DUSP1 rescued p-ERK signaling inhibited by CH. Note: *, $P < 0.05$; **, $P < 0.01$; ***, $P < 0.001$ versus the negative-control group.

the DUSP1 protein in PC-3 cells (Fig. 7B). Furthermore, we treated the cells with BCI, a typical DUSP1 inhibitor. Western blotting demonstrated that knockout or pharmacological inhibition of DUSP1 increased p-ERK expression in PC-3 cells treated with CH (Fig. 7H). Additionally, knockout or pharmacological inhibition of DUSP1 partially enhanced the viability of CH-treated PC-3 cells when compared with control cells (Fig. 7C, I). Moreover, wound healing and transwell assays showed that knockout or inhibition of DUSP1 counteracted the inhibitory effects of CH on the migration of PC-3 cells (Fig. 7D–G). Similar results were obtained for DU145 cells (Fig. S3), suggesting that DUSP1 was involved in the CH-induced downregulation of p-ERK and inhibition of migration in PCa cells.

Effects of CH on PCa xenograft mouse models

Given that CH inhibited PCa cell proliferation and promoted apoptosis by suppressing ERK signaling through upregulation of DUSP1, we assessed the therapeutic potential of CH in vivo using a PC-3 xenograft mouse model. After 7 days of model construction, the mice were randomly divided into the CH and negative-control (DMSO) groups. Each mouse was injected with 30 mg/kg, once every 3 days, whereas DMSO was injected into the negative control mice. After 3 weeks of treatment, CH significantly inhibited tumor growth (Fig. 8A–C), resulting in a 57.96% decrease in tumor volume and a 38.80% decrease in tumor weight (Fig. 8D, E). Immunohistochemical analysis revealed that the expression of Ki-67, a tumor cell proliferation marker, was decreased by approximately 56.65% in the CH group (Fig. 8F, G). Subsequently, western blotting revealed that DUSP1 was upregulated and p-ERK was downregulated in the CH group relative to the negative-control group (Fig. 8H). Altogether, these results suggested that CH suppressed PCa growth by regulating DUSP/ERK signaling in vivo.

Discussion

As the second most common cancer in men, PCa affects approximately 10 million men and leads to more than 400,000 deaths annually worldwide[29]. With consistent advances in research on the pathological mechanisms of PCa, the knowledge regarding novel treatment options has continued to expand[5]. Several signaling pathways have been identified as potential therapeutic targets for PCa. Hyperactivation of PI3K/AKT/mTOR signaling caused by the inactivation of phosphatase and tensin homologue (PTEN) occurs in approximately 20% of primary PCa and 35% of CPRC cases[30]. Therefore, several PI3K/AKT/mTOR inhibitors have been used to treat patients with mCRPC[5]. Traditional Chinese medicine (TCM) is widely used in the treatment of cancer because of its remarkable efficacy and fewer side effects. CH, a Chinese herbal medication, has recently demonstrated excellent efficacy in the treatment of COVID-19. In this study, we preliminarily evaluated the efficacy and mechanism of action of CH in the treatment of PCa. We integrated network pharmacology, molecular docking, and transcriptomic sequencing to investigate the mechanism of action of CH and validated the results through in vitro and in vivo experiments. According to the results, CH holds promise as a novel drug for treating PCa.

Network pharmacological analysis suggested that CH regulated phosphorylation-related biological processes to exert therapeutic effects against PCa (Fig. 1). Based on these results, we evaluated the proliferative ability of CH-treated PCa cells. The results showed that CH significantly inhibited PCa cell viability and induced cell apoptosis. Morphological analysis validated the toxic effects of CH on PCa cells (Fig. 2). In addition, treatment of PCa cells with CH remarkably suppressed cell migration, an important feature of malignant tumors (Fig. 3).

Transcriptomic sequencing showed that ERK1 and ERK2 were potential key targets of CH for the treatment of PCa. The binding between CH and ERK1 or ERK2 was verified via molecular docking (Figs. 4 and 5). In addition, GO analysis showed that DEGs between the CH and DMSO groups were enriched in the negative regulation of ERK1 and ERK2 cascades. Western blotting validated that treatment with CH significantly inhibited p-ERK signaling in PCa cells. Further analysis of the DEGs revealed that DUSPs were upregulated and participated in the negative regulation of ERKs in CH-treated PCa cells. ERK signaling is considered a mature therapeutic target for cancer[27,28]. It is a crucial component of the MAPK signaling pathway and is conserved in almost all eukaryotes[31,32]. It is responsible for delivering extracellular stimuli to the nucleus and inducing a cellular response. DUSP affects phosphorylation involved in signal transduction pathways, thereby regulating a number of important pathways related to cellular metabolism, carcinogenesis, epigenetics and survival[33–37]. Importantly, DUSPs can inhibit the phosphorylation of proteins involved in MAPK signaling, therefore, they are also called MAPK phosphatases (MKPs)[35]. Dysfunction of DUSPs leads to impaired regulation of key molecules in many pathways, especially the MAPK–ERK pathway. It can lead to the inactivation of MAPK1 and MAPK3, resulting in the dephosphorylation of heat shock factor protein 4 and a reduction in its ability to bind to DNA[38]. Moreover, dephosphorylation of p38 can inhibit p38-mediated apoptosis of undifferentiated thyroid cancer cells[39]. Deficiency of DUSPs has been strongly associated with drug resistance in breast cancer. In addition, DUSPs have been identified as novel therapeutic targets for lung cancer and leukemia[33,40,41] This study showed that DUSP/ERK signaling played an important role in the mechanism of action of CH against PCa.

Our study identified cepharanthine hydrochloride (CH) as a novel inhibitor of prostate cancer (PCa) cells through the regulation of the DUSP1/ERK signaling pathway. Similar to a recent study by Guan et al.[42], which demonstrated CH's ability to induce ferroptosis in PCa cells, our findings also underscore CH's anti-tumor potential. However, our work differs by providing a comprehensive mechanistic insight through network pharmacology, transcriptomics, and experimental validation, while also highlighting additional signaling pathways such as MAPK that may contribute to CH's anti-tumor effects, beyond ferroptosis alone.

Finally, several experiments in vivo and in vitro were performed to validate the results of network pharmacology, transcriptomic sequencing, and enrichment analysis. qRT-PCR showed that CH increased the mRNA expression of DUSPs, especially DUSP1 and DUSP10 (Fig. 6). Based on these results, we hypothesized that CH suppressed PCa growth by activating DUSP1 and inhibiting ERK signaling. To verify this speculation, DUSP1 was either knocked out or pharmacologically inhibited in CH-treated PCa cells. The results demonstrated that knockout or inhibition of DUSP1 counteracted the toxic effects of CH on PCa cells (Fig. 7). In addition,

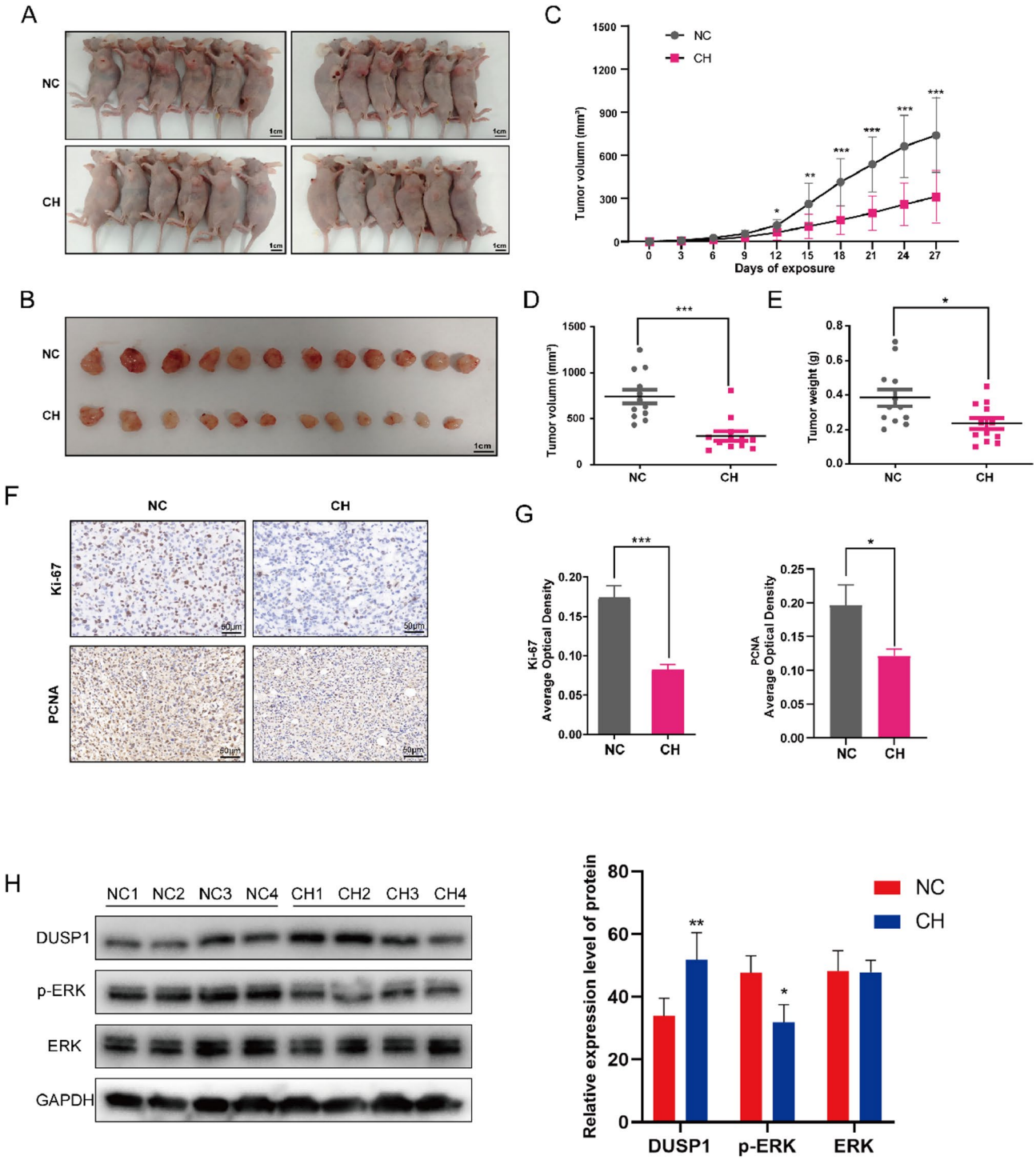

Fig. 8. CH suppressed PCa growth in vivo. (**A**) Tumor detection in nude female mice. (**B**) Morphological features of tumors from the CH and negative-control groups. (**C**) Tumor volume was measured during modeling. (**D**) Tumor volumn was measured after dissection. (**E**) Tumor weight was measured after dissection. (**F**) Immunohistochemical analysis of tumor tissues via Ki-67 and PCNA staining. (**G**) Average optical density of cells positively stained with Ki-67and PCNA. (**H**) DUSP1 and ERK signaling in tumor tissues were detected via western blotting, Each group had four replicates. Note: *, $P<0.05$; **, $P<0.01$; ***, $P<0.001$ versus the negative-control group.

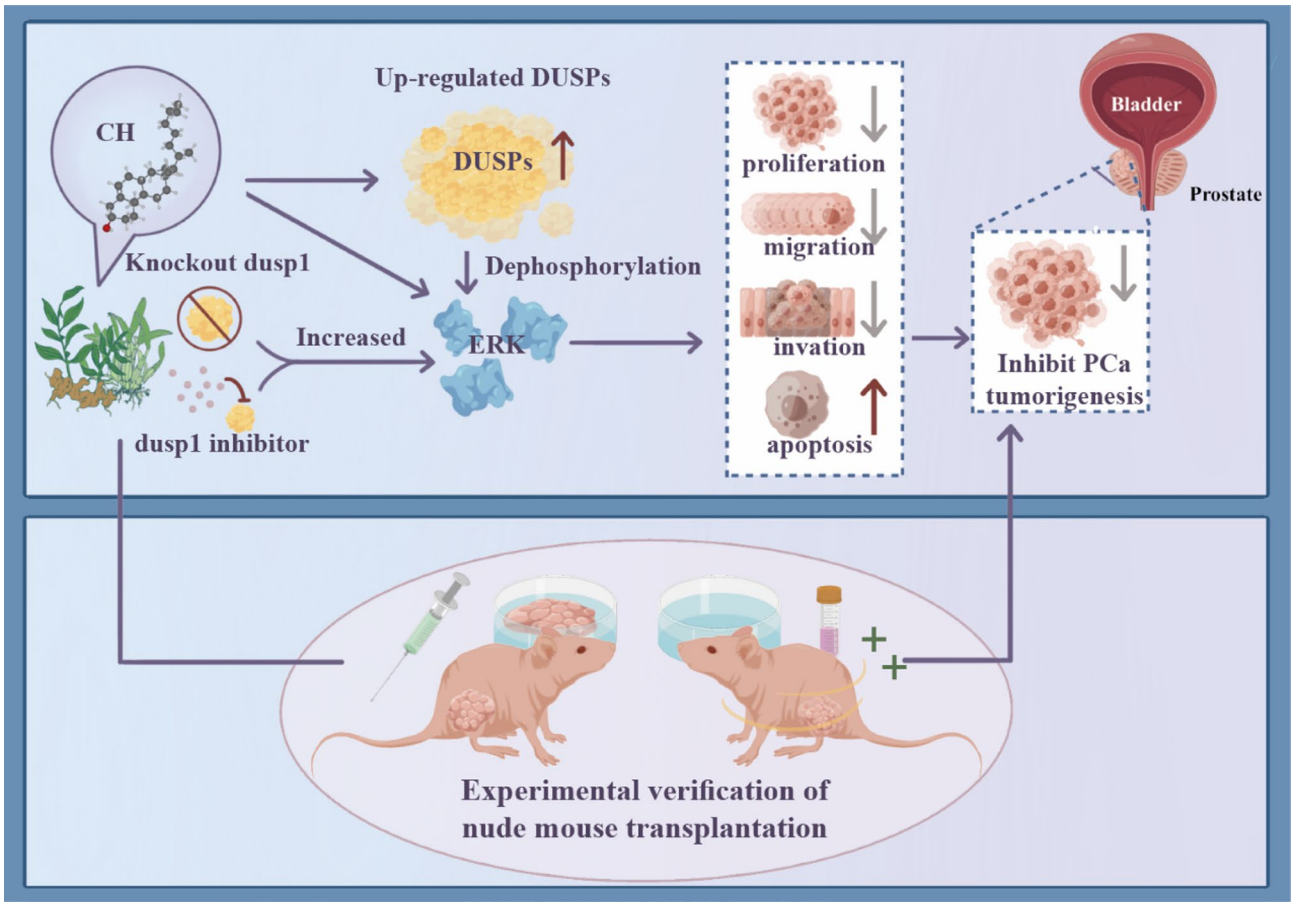

Fig. 9. Schematic diagram demonstrating the mechanism through which CH inhibits tumorigenesis in PCa.

subcutaneous tumor formation experiments in nude mice validated that CH inhibited PCa development in vivo (Fig. 8). Altogether, this study suggests that CH exerts therapeutic effects against PCa by regulating the DUSP/ERK signaling pathway.

While our study demonstrates promising results regarding the anti-tumor effects of cepharanthine hydrochloride (CH) against prostate cancer (PCa) and elucidates its potential mechanism of action through the DUSP1/ERK signaling pathway, several limitations should be acknowledged. First, the experiments were conducted primarily using in vitro cell lines (PC-3 and DU145) and an in vivo xenograft mouse model, which may not fully capture the complexity of human PCa. Further clinical trials are needed to validate the efficacy and safety of CH in human patients. Additionally, the molecular mechanisms underlying the interaction between CH and its targets, particularly the specific binding sites and dynamics within the ERK1/2 proteins, warrant further investigation using more advanced techniques such as crystallography or nuclear magnetic resonance (NMR) spectroscopy. Moreover, the study focused on a limited number of cell lines and signaling pathways, and a broader screening of PCa cell lines and signaling networks may reveal additional targets and mechanisms of action for CH. Finally, while the results suggest that CH upregulates DUSP1 and suppresses ERK phosphorylation, the specific downstream effects of this signaling cascade on PCa progression and patient outcomes remain to be elucidated.

Conclusion

In conclusion, this study reveals that CH is a potent inhibitor of PCa cell proliferation and migration. According to the results of network pharmacology, CH may exert therapeutic effects against PCa by regulating protein phosphorylation. Transcriptomic sequencing highlighted the involvement of ERK signaling and DUSPs in the anti-tumor effects of CH. Molecular docking suggested similar and strong binding between CH and ERK1 or ERK2. Treatment with CH upregulated DUSP1 and suppressed ERK phosphorylation, eventually inhibiting the growth of PCa (Fig. 9). Knockout and pharmacological inhibition of DUSP1 partially reversed the CH-induced toxicity in PCa cells in vitro. Additionally, CH effectively suppressed tumorigenesis in nude mice with PCa. These results suggest that CH serves as a promising drug for treating PCa, which may act by regulating DUSP1/ERK signaling in PCa cells.

Data availability

The datasets generated during the current study are available in the Gene Expression Omnibus (GEO), GSE287711. The data presented in this study are available on request from the corresponding author.

Received: 18 December 2024; Accepted: 19 May 2025
Published online: 24 May 2025

References

1. Siegel, R. L., Giaquinto, A. N. & Jemal, A. Cancer statistics, 2024. *CA Cancer J. Clin.* **74**, 12–49. https://doi.org/10.3322/caac.21820 (2024).
2. Zheng, R. S. et al. Cancer incidence and mortality in China, 2022. *Zhonghua Zhong Liu Za Zhi Chin. J. Oncol.* **46**, 221–231. https://doi.org/10.3760/cma.j.cn112152-20240119-00035 (2024).
3. Martin-Caraballo, M. Regulation of molecular biomarkers associated with the progression of prostate cancer. *Int. J. Mol. Sci.* **25**, 4171. https://doi.org/10.3390/ijms25084171 (2024).
4. Hussain, M. et al. Metastatic hormone-sensitive prostate cancer and combination treatment outcomes: A review. *JAMA Oncol.* **10**, 807–820. https://doi.org/10.1001/jamaoncol.2024.0591 (2024).
5. He, Y. et al. Targeting signaling pathways in prostate cancer: Mechanisms and clinical trials. *Signal Transduct. Target. Ther.* **7**, 198. https://doi.org/10.1038/s41392-022-01042-7 (2022).
6. Cavada, B. S. et al. Lectins applied to diagnosis and treatment of prostate cancer and benign hyperplasia: A review. *Int. J. Biol. Macromol.* **190**, 543–553. https://doi.org/10.1016/j.ijbiomac.2021.09.011 (2021).
7. Bryce, A. H., Sartor, O. & de Bono, J. DNA repair and prostate cancer: A field ripe for harvest. *Eur. Urol.* **78**, 486–488. https://doi.org/10.1016/j.eururo.2020.06.020 (2020).
8. Sharma, P. et al. Nivolumab plus ipilimumab for metastatic castration-resistant prostate cancer: Preliminary analysis of patients in the checkmate 650 trial. *Cancer Cell* **38**, 489-499.e483. https://doi.org/10.1016/j.ccell.2020.08.007 (2020).
9. Guerrero-Ochoa, P. et al. Prostate cancer and the mevalonate pathway. *Int. J. Mol. Sci.* **25**, 2152. https://doi.org/10.3390/ijms25042152 (2024).
10. Desgrouas, C. et al. Ethnobotany, phytochemistry and pharmacology of Stephania rotunda Lour. *J. Ethnopharmacol.* **154**, 537–563. https://doi.org/10.1016/j.jep.2014.04.024 (2014).
11. Chen, Y. et al. Antiviral drugs screening for swine acute diarrhea syndrome coronavirus. *Int. J. Mol. Sci.* **23**, 11250. https://doi.org/10.3390/ijms231911250 (2022).
12. Rogosnitzky, M. & Danks, R. Therapeutic potential of the biscoclaurine alkaloid, cepharanthine, for a range of clinical conditions. *Pharmacol. Rep. PR* **63**, 337–347. https://doi.org/10.1016/s1734-1140(11)70500-x (2011).
13. Furusawa, S. & Wu, J. The effects of biscoclaurine alkaloid cepharanthine on mammalian cells: implications for cancer, shock, and inflammatory diseases. *Life Sci.* **80**, 1073–1079. https://doi.org/10.1016/j.lfs.2006.12.001 (2007).
14. Liu, B. & Deng, J. X. Effect of cepharanthine on the stemness of lung squamous cell carcinoma based on network pharmacology and bioinformatics. *Biomed. Res. Int.* **2022**, 5956526. https://doi.org/10.1155/2022/5956526 (2022).
15. Shahriyar, S. A., Woo, S. M., Seo, S. U., Min, K. J. & Kwon, T. K. Cepharanthine enhances TRAIL-mediated apoptosis through STAMBPL1-mediated downregulation of survivin expression in renal carcinoma cells. *Int. J. Mol. Sci.* **19**, 3280. https://doi.org/10.3390/ijms19103280 (2018).
16. Kogure, K. et al. Potent antiperoxidation activity of the bisbenzylisoquinoline alkaloid cepharanthine: The amine moiety is responsible for its pH-dependent radical scavenge activity. *Biochem. Biophys. Acta.* **1426**, 133–142. https://doi.org/10.1016/s0304-4165(98)00146-9 (1999).
17. Samra, Y. A. et al. Cepharanthine and Piperine ameliorate diabetic nephropathy in rats: Role of NF-κB and NLRP3 inflammasome. *Life Sci.* **157**, 187–199. https://doi.org/10.1016/j.lfs.2016.06.002 (2016).
18. Li, S. et al. Transcriptome analysis of cepharanthine against a SARS-CoV-2-related coronavirus. *Brief. Bioinform.* **22**, 1378–1386. https://doi.org/10.1093/bib/bbaa387 (2021).
19. Zhang, S. et al. Comparison of viral RNA-host protein interactomes across pathogenic RNA viruses informs rapid antiviral drug discovery for SARS-CoV-2. *Cell Res.* **32**, 9–23. https://doi.org/10.1038/s41422-021-00581-y (2022).
20. Biswas, K. K. et al. Cepharanthine triggers apoptosis in a human hepatocellular carcinoma cell line (HuH-7) through the activation of JNK1/2 and the downregulation of Akt. *FEBS Lett.* **580**, 703–710. https://doi.org/10.1016/j.febslet.2005.12.048 (2006).
21. Rattanawong, A. et al. Cepharanthine exhibits a potent anticancer activity in p53-mutated colorectal cancer cells through upregulation of p21Waf1/Cip1. *Oncol. Rep.* **39**, 227–238. https://doi.org/10.3892/or.2017.6084 (2018).
22. Gao, S., Li, X., Ding, X., Qi, W. & Yang, Q. Cepharanthine induces autophagy, apoptosis and cell cycle arrest in breast cancer cells. *Cell. Physiol. Biochem. Int. J. Exp. Cell. Physiol. Biochem. Pharmacol.* **41**, 1633–1648. https://doi.org/10.1159/000471234 (2017).
23. Xu, W. et al. Tetrandrine and cepharanthine induce apoptosis through caspase cascade regulation, cell cycle arrest, MAPK activation and PI3K/Akt/mTOR signal modification in glucocorticoid resistant human leukemia Jurkat T cells. *Chem. Biol. Interact.* **310**, 108726. https://doi.org/10.1016/j.cbi.2019.108726 (2019).
24. Kanehisa, M., Furumichi, M., Sato, Y., Kawashima, M. & Ishiguro-Watanabe, M. KEGG for taxonomy-based analysis of pathways and genomes. *Nucleic Acids Res.* **51**(D1), D587–D592 (2023).
25. Liu, X., Cui, S., Li, W., Xie, H. & Shi, L. Elucidation of the anti-colon cancer mechanism of Phellinus baumii polyphenol by an integrative approach of network pharmacology and experimental verification. *Int. J. Biol. Macromol.* **253**, 127430. https://doi.org/10.1016/j.ijbiomac.2023.127429 (2023).
26. Grogan, L. & Shapiro, P. Progress in the development of ERK1/2 inhibitors for treating cancer and other diseases. *Adv. Pharmacol (San Diego, Calif.)* **100**, 181–207. https://doi.org/10.1016/bs.apha.2024.04.001 (2024).
27. Maik-Rachline, G., Hacohen-Lev-Ran, A. & Seger, R. Nuclear ERK: Mechanism of translocation, substrates, and role in cancer. *Int. J. Mol. Sci.* **20**, 1194. https://doi.org/10.3390/ijms20051194 (2019).
28. Fu, L., Chen, S., He, G., Chen, Y. & Liu, B. Targeting extracellular signal-regulated protein kinase 1/2 (ERK1/2) in cancer: An update on pharmacological small-molecule inhibitors. *J. Med. Chem.* **65**, 13561–13573. https://doi.org/10.1021/acs.jmedchem.2c01244 (2022).
29. Sung, H. et al. Global Cancer Statistics 2020: GLOBOCAN estimates of incidence and mortality worldwide for 36 cancers in 185 countries. *CA Cancer J. Clin.* **71**, 209–249. https://doi.org/10.3322/caac.21660 (2021).
30. Jamaspishvili, T. et al. Clinical implications of PTEN loss in prostate cancer. *Nat. Rev. Urol.* **15**, 222–234. https://doi.org/10.1038/nrurol.2018.9 (2018).
31. Chang, L. & Karin, M. Mammalian MAP kinase signalling cascades. *Nature* **410**, 37–40. https://doi.org/10.1038/35065000 (2001).
32. Lavoie, H., Gagnon, J. & Therrien, M. ERK signalling: A master regulator of cell behaviour, life and fate. *Nat. Rev. Mol. Cell Biol.* **21**, 607–632. https://doi.org/10.1038/s41580-020-0255-7 (2020).
33. Masiero, M. et al. Notch3-mediated regulation of MKP-1 levels promotes survival of T acute lymphoblastic leukemia cells. *Leukemia* **25**, 588–598. https://doi.org/10.1038/leu.2010.323 (2011).
34. Mutlak, M. & Kehat, I. Dual specific phosphatases (DUSPs) in cardiac hypertrophy and failure. *Cell. Signal.* **84**, 110033. https://doi.org/10.1016/j.cellsig.2021.110033 (2021).

35. Pulido, R. & Lang, R. Dual specificity phosphatases: From molecular mechanisms to biological function. *Int. J. Mol. Sci.* **20**, 4372. https://doi.org/10.3390/ijms20184372 (2019).
36. Dang, H. et al. Pin1 inhibitor API-1 sensitizes BRAF-mutant thyroid cancers to BRAF inhibitors by attenuating HER3-mediated feedback activation of MAPK/ERK and PI3K/AKT pathways. *Int. J. Biol. Macromol.* **248**, 125867. https://doi.org/10.1016/j.ijbiomac.2023.125867 (2023).
37. Liu, C. et al. Dual-specificity phosphatase DUSP1 protects overactivation of hypoxia-inducible factor 1 through inactivating ERK MAPK. *Exp. Cell Res.* **309**, 410–418. https://doi.org/10.1016/j.yexcr.2005.06.022 (2005).
38. Yu, W. et al. A novel amplification target, DUSP26, promotes anaplastic thyroid cancer cell growth by inhibiting p38 MAPK activity. *Oncogene* **26**, 1178–1187. https://doi.org/10.1038/sj.onc.1209899 (2007).
39. Balko, J. M. et al. Profiling of residual breast cancers after neoadjuvant chemotherapy identifies DUSP4 deficiency as a mechanism of drug resistance. *Nat. Med.* **18**, 1052–1059. https://doi.org/10.1038/nm.2795 (2012).
40. Moncho-Amor, V. et al. DUSP1/MKP1 promotes angiogenesis, invasion and metastasis in non-small-cell lung cancer. *Oncogene* **30**, 668–678. https://doi.org/10.1038/onc.2010.449 (2011).
41. Hou, M. F. et al. Decreased total MKP-1 protein levels predict poor prognosis in breast cancer. *World J. Surg.* **36**, 1922–1932. https://doi.org/10.1007/s00268-012-1608-y (2012).
42. Guan, J. S. et al. Cepharanthine hydrochloride: A novel ferroptosis-inducing agent for prostate cancer treatment. *Front. Pharmacol.* **16**, 1536375. https://doi.org/10.3389/fphar.2025.1536375 (2025).

Acknowledgements

We thank for the Lian Chuan Technology Co., Ltd., Hangzhou to do RNA transcriptomics analysis for us.

Author contributions

Zongming Dong，Xiaosa Chang and Luo Xing Writing the main manuscript text .Zongming Dong, Xiaosa Chang, Zeyu Huang, Yingbing Wu, Yu Chen Visualization.Zongming Dong, Xiaosa Chang, Zeyu Huang, Yu Chen Software.Zongming Dong, Xiaosa Chang, Hui Li, Xing Luo, Ming Deng, Tingting Chen, Bishao Sun, Ronghua Wu, Qingjian Wu Data curation.Zongming Dong, Xiaosa Chang, Hui Li, Xing Luo, Ronghua Wu Methodology.Zongming Dong，Hui Li，Ming Deng，Bishao Sun，Qingjian Wu Formal analysis.Ji Zheng，–Jingzhen Zhu，Hui Li，Tingting Chen Investigation.Ji Zheng，Jingzhen Zhu Resources, Supervision, Project administration, Investigation, Funding acquisition. All authors reviewed the manuscript.

Funding

This study was supported by the Top Young and Middle-aged Medical Talent of Chongqing (Ji Zheng), the "Red Doctor" talent program of Army Medical University (Jingzhen Zhu), Young Doctor talent incubation program project of Army Military Medical University Xinqiao hospital, (Grant No. 2023YQB035, Jingzhen Zhu), the Young PhD Incubation Program of The second affiliated hospital of Army Medical University (Grant No. 2022YQB047, Qingjian Wu), Chongqing Science and Health Joint Fund Program for Young and Middle-aged Top-Notch Talents (Grant No. 2023GDRC007, Ji Zheng).

Declarations

Competing interests

The authors declare no competing interests.

Additional information

Supplementary Information The online version contains supplementary material available at https://doi.org/10.1038/s41598-025-03004-9.

Correspondence and requests for materials should be addressed to J.Z. or J.Z.